Materials Science-Poland, 40(1), 2022, pp. 101-115
http://www.materialsscience.pwr.wroc.pl/
DOI: 10.2478/msp-2022-0013

Underwater friction-stir welding of a stir-cast AA6061-SiC metal matrix composite: optimization of the process parameters, microstructural characterization, and mechanical properties

Ibrahim Sabry[1,*], A.M. Hewidy[1,2]

[1]Faculty of Engineering, Benha University, Department of Mechanical Engineering, Egypt
[2]Manufacturing Engineering Department, Modern Academy for Engineering and Technology, P.O. Box, Cairo 11571, Egypt

It is an underlying fact for the case of the joining process especially welding to have optimized parameters to achieve joints with outstanding mechanical characteristics. In the current article, using stir-cast aluminum-based alloy (Al 6061) is stir-cast with Al 6061/5%wt. silicon carbide, Al 6061/10%wt. silicon carbide, and Al 6061/18%wt. silicon carbide was welded using an underwater friction-stir welding process. Optimum welding parameters [namely, tool rotating speed (N), welding speed (S), and silicon carbide (SiC)] are investigated using analysis of variance (ANOVA) and response surface methodology (RSM) statistical approaches. High ultimate tensile strength and microhardness were set as required characteristics of quality welds. Since there are two responses and two objectives, multiple-criteria decision-making approach—response surface methodology was performed alongside ANOVA. Optimal parameters from these statistical approaches are converged to a tool rotating speed of 1,736.36 rpm, a welding speed of 11.58 mm/min, and a SiC of 16.67%, respectively. For the current inquiry, the computed ultimate tensile strength and microhardness are 984 MPa and 89.9 HV, respectively, and these values are congruent with the findings of effectiveness studies. It is deduced from this study that the optimal parameters are convergent irrespective of the two used techniques for the investigated experimental data.

Keywords: *UWFSW, UTS, MHV, RSM, optimization, desirability approach*

Abbreviations: *AA, aluminum alloy; AMC, aluminum matrix composite; BM, base metal; FSW, friction-stir welding; HAZ, heat affected zone; HV, vickers hardness; NZ, nugget zone; RSM, response surface methodology; TMAZ, thermomechanically affected zone; UTS, lutimate tensile strength; UWFSW, underwater friction-stir welding; WNH, weld nugget hardness*

1. Introduction

Friction-stir (FS) welded aluminum matrix composite (AMC) joints are used in the automotive, naval, and aeronautical industries because of their appealing properties such as altitude strength, depress density, superb corrosion resistance, preferable thermal conductivity, depressed expansion of thermal, and preferable dimensional stability by perfect strength-to-mass ratio [1]. The interaction of matrix and encouragement particles in the pool of molten weld causes subaltern brittle phases in the molten pool of the weld or reinforcement collapse in the pool of molten metal, making AMC a quixotic material for application in modern obstetrics [2]. FSW is a less costly and more effective solid-state welding procedure for AMCs to generate efficient defect-free welds (reduced cracking, minimal deformation, lower porosity, etc.) [1]. Many researchers have begun and continue their studies in the sectors of aviation, aerospace, automotive, and shipbuilding because of the appealing properties of FSW. To improve the performance of the FS-welded joints, they are developing enhanced procedures and newer materials for the base matrix and reinforcement. For the optimization of maximal mechanical characteristics, advanced approaches such as UTS, WHN, and others are required. RSM is one of the most precise methods for selecting the best welding settings with the least amount of time, material, and labor [3].

* E-mail: ibrahim.sabry@bhit.bu.edu.eg

El-Kassas et al. [4] documented that given an optimum set of welding conditions, characterized by a rotation speed of 1,800 rpm, a welding speed of 1 mm/min, a penetration depth of 2 mm, and a tool with a cylindrical-conical pin profile, FS-welded joints showed an excellent strength, in comparison with the strengths achieved resultant to using other combinations of welding conditions. Recent research has revealed that T-joints, which are commonly seen in mechanical constructions, may be fused utilizing FS welding [5]. However, in certain regions, UFSW of complicated components should still be investigated. As a result, if UFSW proves to be more useful than standard FSW, it will have a significant influence on the welding industry, helping to improve technology. As a result, given the current situation, the application of UWFSW on AA 6063 pipes, as well as examination, is critical. The friction-stir welding procedure is linked to several problems. Tunneling, wormholes, voids, flash, kissing bonds, surface galling, porosity, lack of fill, lack of penetration, and other factors reduce the strength of a structure. Mechanical property degradation frequently leads to premature failure with little warning. However, as compared to FSW, UWFSW is less prone to these flaws [6]. Sabry et al. [7] documented that multi-objective optimization of the UWFSW process was a desirable feature because UWFSW had a high UTS of 218 MPa and a nugget zone hardness of 83 VHN compared to 201 MPa and 65 VHN for the traditional process. Researchers have successfully welded and studied plates and pipes constructed of aluminum alloys such as Al AA 6063-T6 [8], Al 6063 [9], Al 6061 [10], Al 1050 [11], and Al 1050 [12]. In comparison to traditional FSW, a high rotating speed does not influence the heat generated in UWFSW, according to the main findings. In the case of UWFSW, a balanced thermal cycle provides an extra benefit. High travel and tool rotating speeds are now suggested for UWFSW [13]. There is a dearth of literature on welding pipes with the UWFSW technique. Resistance welding, inert metal gas welding [14], inert tungsten gas welding, and other welding techniques are used in an industrial setting. Jandaghi et al.'s [15] study dealt with improvement of the mechanical strength of aluminum joints formed by friction-stir welding (FSW), and a post-weld heat treatment comprising solution treatment and subsequent aging (STA) is extensively used in their research. Aerospace aluminum alloys AA2198 and AA7475 were FSW-ed in such a way that the results were physically indistinguishable, and the resultant welded products in their different states were used in this investigation. The precipitation strengthening with the aging of welded specimens was studied using differential scanning calorimetry (DSC). The DSC results were used to construct the post-weld aging methods. As a result, welded sheets were solution treated for 10–90 min at 480°C and 540°C, and then air-cooled and aged for 2–40 h at 155°C and 170°C, respectively. Optical micrographs demonstrated that greater homogenizing temperature led to nucleation of finer grains from high stress localized spots in the stir zone (SZ) and TMAZ by a quicker growth rate due to faster recrystallization kinetics.

At SZ and TMAZ of AA7475, increased solution-treatment duration and temperature resulted in the buildup of Cu-enriched intermetallic phases in the grain boundaries, weakening of grain adhesion, and sample failure. In the as-welded state, the hardness of the AA7475 alloy rose, while the hardness of the AA2198 alloy decreased. In AA2198, post-weld heat treatment increased hardness, but in AA7475, it decreased. The grain size, on the other hand, was unaffected. In the research of Jandaghi et al. [16], dissimilar FSW sheets AA2198-AA7475 and AA2198-AA6013 were solution treated for 1 h at 460–580°C. Both dissimilar weldments on the AA2198 side were completely degraded after annealing at 580°C. Solution treatment caused abnormal grain growth in the stir zone (SZ), and higher treatment temperatures increased the fraction of transformed grains, according to microstructure inspection. The pre-melting of grain boundaries (GBs) at 540°C aided the diffusion of solute atoms to the GBs, according to SEM analysis. Massive Cu diffusion to the GBs resulted in Cu-rich eutectic phases in AA7475 and AA2198, as well as dense Cu-rich particles in AA6013. In the research of Jandaghi et al. [17], post-weld heat treatment (PWHT) of dissimilar AA7475-AA2198

Table 1. The chemical make-up of 6061 Al-alloy

Element	Mg	Si	Fe	Cu	Mn	Zn	Cr	Ti	Al
Wt.%	1.1	0.55	0.4	0.10	0.9	0.25	0.04	0.12	Remainder

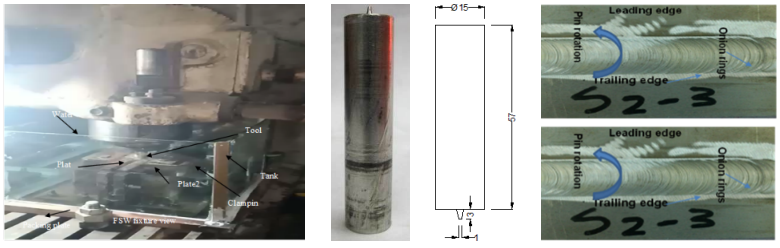

(A) (B) (C) (D)

Fig. 1. Schematic representation of UWFSW **(A)** UWFSW welding fixture. **(B)** Photo of a tool **(C)** tool dimension **(D)** specimens of 6061/18% SiC AMC

FSW was performed at 560°C, followed by water-quenching. Microstructural analyses demonstrated that the composition difference at high-temperature solution treatment was the driving force for Cu diffusion from advancing AA2198 via grain boundary liquid-metal thin-films, resulting in adequate intergranular segregation of the Cu-Zn phase. Intergranular failure has been linked to weld residual stresses, poor interfacial strength, grain boundary transition, and wetting, as well as thermal expansion coefficient disparities. Numerous studies are researches that aim to improve the responses (UTS, WNH, etc.) of FSW joints made of various aluminum alloys reinforced with various ceramic particles by selecting appropriate process parameters and employing newer methods on newer and advanced materials. The goal of this research is to produce a novel hybrid composite comprised of AA6061 as a base material and reinforced with SiC to improve the mechanical and metallurgical features of UWFS-welded joints. The RSM and desirability techniques were used to establish empirical correlations between UWFSW parameters (N, S, and SiC) and the two responses (UTS and WNH), as well as to select the best welding circumstances for UWFSW joints with optimal UTS and WNH.

2. Experimental work

2.1. Materials and method

Aluminum alloy was employed as a matrix material. Because of its strong corrosion resistance, great machining qualities, low weight, and ductility, the aluminum alloy was chosen. The alloy Al 6061 is mostly utilized in the aerospace sector. 6061/SiC AMC was employed in this study, as well as UWFSW 6061 alloy enhancement together with SiC particles. The matrix is a standard 6061 aluminum alloy with the specified chemical composition, as provided in Table 1. The stir-casting approach was used to generate SiC enhancement 6061 matrix composites in a top-loading electric resistance muffle furnace, as indicated in the literature [1]. The average size of the SiC particles was 400 mesh (40 m). Castings were reinforced with 5 SiC wt.%, 10 SiC wt.%, and 18 SiC wt.% scale (150 mm $\times$ 750 mm $\times$ 10 mm) composite specimens that have already been slashed, cleaned, and butt-welded along the joint line for UWFSW.

The geometrical dimensions are shown in Figure 1. The conical pin was designed to facilitate piercing the tool to the specimens as straightforwardly as possible during the welding process. The welding experiments were performed on an automated vertical milling machine with a custom-made fixture to clamp the welding plates, as shown in Figures 1B and 1C.

2.2. Metallographic and macrostructure studies

Following the standard metallographic procedure, mirror polishing and etching with Keller's reagent (HCL + HF + HNO_3 + distilled water) were performed. The metallographic specimens were made from 6061 AMC and 6061 AMC that had been welded together. According to ASTM E8-04, the standard tensile specimens were sliced perpendicular to the joint line and created from all specimens [18]. TS has been prepared by the length of a gauge of 57.2 mm, the width of a gauge of 12.2 mm, and a thickness of 10 mm. The tensile specimens were done using a Blue Star universal tensile testing machine (SE UTE 200) with an extreme capacity of 200kN, as indicated in Figure 2. A Chinese-made optical scanning microscope was used to examine the microstructure of UWFS-welded specimens (XPZ-830 T) [16]. In the same way, the Al-matrix stir cast as a composite cast aluminum matrix and the welded junction were microstructurally examined. The UWFS-welded and other specimens were MHV using the FIE model VM50 VH tester. VH measurements were taken at various locations on both sides of the weld zone under a constant load of 0.8 kgf for a dwell period of 17 s. The hardness data were then categorized as average microhardness [17, 19].

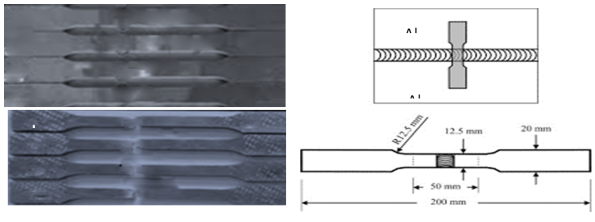

Fig. 2. **(A)** Photos of the specimens after tensile test. **(B)** Photos of the specimens before tensile test. **(C)** Dimensions of tensile test specimens (dimensions are in millimeter)

3. Surface response modeling and optimization

Researchers and engineers are continually trying to figure out what input process parameters or characteristics will result in the best output response. The optimal values are either the extreme or minimal of a function, depending on the input process parameters. RSM is an essential mathematical and statistical approach for constructing an empirical model. Independent variables can be quantitatively stated in both industrial and experimental situations, as demonstrated in Eq. (1). These independent parameters can thus have the following functional relationship:

$$X = \gamma(Y_1; Y_2; Y_3; Y_n) \pm error\ from\ experiments \quad (1)$$

The response surface or function is the relationship between the response, X, and the quantitative parameters, Y_1, Y_2, Y_3, …, Y_n. The response surface reacts to the collection of independent parameters that are provided. A typical surface is generated for a given set of independent factors. For unknowns inside the experimental range, a polynomial approximation can be done satisfactorily. The RSM was used in this study to develop a mathematical model for friction-stirred joining of AA6061/SiC and to determine the quality parameters of weldments using multiple regression equations. The independent parameter is treated as a surface for which a mathematical model is fitted when using the RSM. The functions of N, S, and SiC are the UTS and WNH of the UWFSW of AA6061/SiC. The following is a description of the surface:

$$\mathrm{UTS} = f(\mathrm{N}; \mathrm{S}; \mathrm{SiC}) \quad (2)$$

$$\mathrm{WNH} = f(\mathrm{N}; \mathrm{S}; \mathrm{SiC}) \quad (3)$$

The response surface is represented by the second-order regression equation:

$$X = a_0 + \sum a_i x_i + \sum a_{ij} x_i x_j + \sum a_{ii} {x_i}^2 + \varepsilon \quad (4)$$

The X response surface was shown using second-order polynomial regression, where a_0 is the average response, and a_i, a_{ii}, and a_{ij} are coefficients based on the main and interaction effects of the parameters.

Table 2. UWFSW process parameters and their limits

	Level		
Parameter	**−1**	**0**	**1**
Silicon carbide (SiC) (%)	5	10	18
Rotation speed (*N*) (rpm)	1,000	1,400	1,800
Travel speed (*S*) (mm/min)	10	20	30

During the UWFSW of AA6061/SiC, three process parameters with three levels have been considered in this study: N, S, and SiC. Before actual welding, the correlation of process parameters with UTS and WNH of welded joints is usually developed in the design. The Box–Behnken design technique was utilized in this study to develop the correlation and determine the best design parameters for improving the UTS and WNH of UWFS-welded connections.

As a three-factorial for determining the correlation between the response parameters (UTS and WNH) and the input parameters, a Box–Behnken experimental design was chosen (N, S, and SiC). Table 2 shows the most influential UWFSW process factors on output responses, along with their levels, as determined using the Box–Behnken model design. −1 (low), 0 (middle), and 1 (high) are the levels of the process parameters (high). Table 3 shows that the design matrix for a total of 27 tests is required, according to the Box–Behnken experimental design.

One of the most often used strategies for multiple response optimization procedures is the desirability approach. The fundamental benefit of the desirability method is that it assigns value to every response, such as UTS or WNH. It turns these single replies into the desirability function, a dimensionless parameter that gives integers between 0 and 1. The overall desirability function converts numerous answers such as UTS and WNH into a dimensionless measure of performance. Multiple responses, such as UTS and WVH, are turned into a dimensionless measure in this study. Eq. (5) gives the total desirability function:

$$\begin{aligned} &Desirability\ function; \\ &F = (d_1 * d_2 * d_1 * d_n)^{\frac{1}{2}} \end{aligned} \tag{5}$$

Table 3. Full factorial design matrix

Run	**SiC**	***N***	***S***	**UTS (MPa)**	***VHN*ode**
				code	
1	5	1,000	10	205.00	64.544
2	10	1,000	10	196.00	55.243
3	18	1,000	10	190.00	52.942
4	5	1,000	20	200.00	55.980
5	10	1,000	20	190.00	53.679
6	18	1,000	20	180.00	51.378
7	5	1,000	30	190.00	55.198
8	10	1,000	30	185.00	52.897
9	18	1,000	30	174.00	50.596
10	5	1,400	10	202.00	56.113
11	10	1,400	10	186.40	53.812
12	18	1,400	10	174.70	51.511
13	5	1,400	20	195.30	54.548
14	10	1,400	20	183.70	52.247
15	18	1,400	20	172.30	49.946
16	5	1,400	30	193.10	53.766
17	10	1,400	30	180.03	51.465
18	18	1,400	30	170.32	49.164
19	5	1,800	10	196.00	56.113
20	10	1,800	10	185.10	52.380
21	18	1,800	10	176.20	50.079
22	5	1,800	20	191.30	53.117
23	10	1,800	20	184.20	50.816
24	18	1,800	20	171.20	48.515
25	5	1,800	30	187.10	52.335
26	10	1,800	30	181.10	50.034
27	18	1,800	30	166.30	47.732

where d_n denotes the response's desirability and n denotes the number of responses.

Design-Expert software is utilized to optimize the UWFSW process parameters. By establishing the intended goals for each input parameter and response, both numerical and graphical optimization approaches are used. All of the goals are incorporated into the overall desirability function throughout the numerical optimization process. This procedure optimizes the objective function by determining the maximum and lowest limits for each element and determining the response that will maximize the objective function. This graphical approach is utilized to identify the interaction effects of process factors on replies in graphical optimization with multiple responses, and it is represented using 2D and 3D contour plots. When dealing with a large number of replies, numerical optimization

should be used initially to define a feasible region, while graphical optimization may be used to depict a viable response area, and the shaded zone reflects the unsuitable optimization criterion. The flow chart for the Design-Expert software's optimization process is shown in Figure 3.

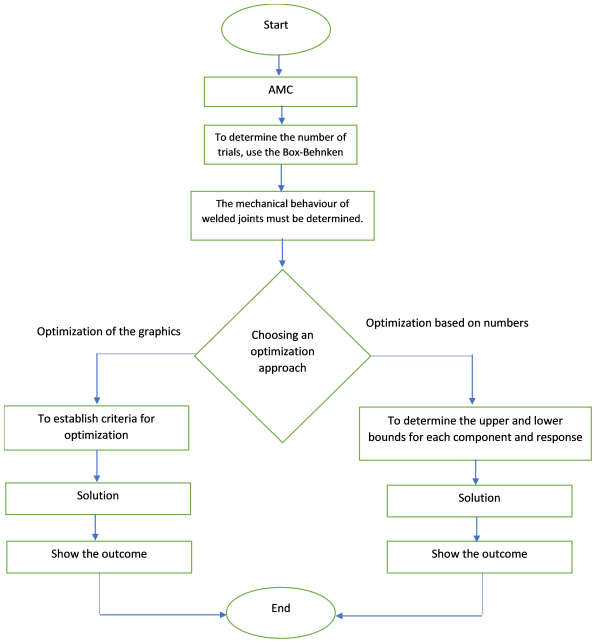

Fig. 3. Experimentation flowchart of the UWFSW

4. Results and discussion

4.1. Mechanical properties

The surface finishing for each UWFSW specimen of Al 6061/18% SiC gave a smooth weld surface without lateral flash; meanwhile Al 6061/5% SiC shows an unsmooth weld surface condition. Based on observation, we can infer that this is the relation between rotation speed, travel speed, the ratio of SiC, and flash occurrence. The lower values of rotation, travel speed, and SiC 18% resulted in an absence of lateral flash. In lieu, the decrease in SiC may direct to the presence of lateral flash. Hence, it explains that the welding particulars may influence the character of the external surface. Tensile specimens have been prepared in standard dimensions according to ASTM E8 as shown in Figure 2 and tested using the universal testing machine. A Santam STM-50 machine has been used to evaluate tensile properties. The testing machine had a crosshead speed of 5 mm/min. During the test, stress and strain have been recorded simultaneously, as shown in Figure 4 and Figure 5. The maximum UTS and YS have been obtained for specimens produced by Al 6061/18% SiC. The corresponding combination of tool rotational speed and travel speed has been 1,800 rpm and SiC 18%, respectively. The UTS and the YS have been 228 MPa and 140.3 MPa, respectively, which have been 91.2% and 92.3% of the base material.

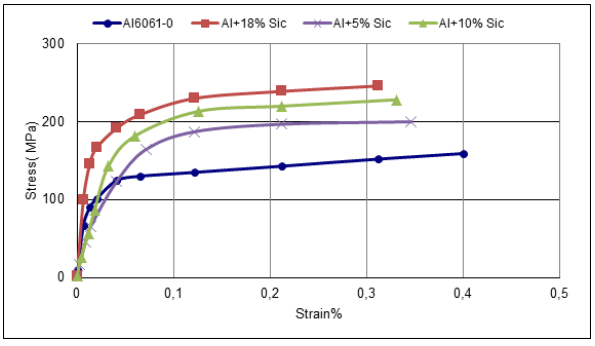

Fig. 4. Stress–strain curve of unwelded AA 6061 Al-SiC alloy specimens from the tensile test

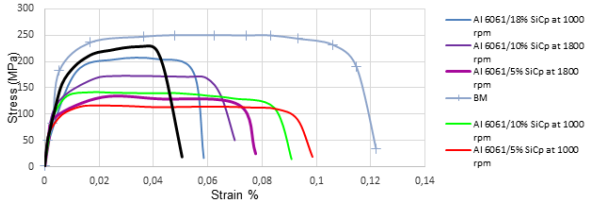

Fig. 5. Stress-strain curve of welded AA 6061 Aluminium-silicon carbide alloy specimens from the tensile test for weld speed 10 mm/min

Table 2 shows how the Box–Behnken model is used to create an experimental design matrix. FSW on hybrid composites was carried out by varying process parameters such as N, S, and SiC following the experimental design matrix provided in Table 3. According to ASTM standards, test specimens for the tensile and VH tests were made using manufactured welded joints. To create the empirical mathematical relationships, UTS and WNH

Table 4. ANOVA results for UTS

Exporter	Squares of sum	df	Square of mean	*F*-value	*p*-value	
Model	2,637.03	9	293.00	52.07	<0.0001	Significant
A-SiC	1,896.87	1	1,896.87	337.08	<0.0001	
B-N	73.62	1	273.62	48.62	<0.0001	
C-S	397.11	1	397.11	70.57	<0.0001	
AB	6.56	1	6.56	1.17	0.2952	
AC	1.37	1	1.37	0.24	0.6285	
BC	30.72	1	30.72	5.46	0.0320	
A^2	47.11	1	47.11	8.37	0.0101	
B^2	19.92	1	19.92	3.54	0.0771	
C^2	0.10	1	0.10	0.018	0.8943	
Residual	95.66	17	5.63			
Cor Total	2,732.69	26				

Table 5. ANOVA results for microhardness

Exporter	Squares of sum	df	Square of mean	*F*-value	*p*-value	
Model	260.47	*9*	28.94	21.80	<0.0001	Significant
A-SiC	138.06	1	138.06	104.02	<0.0001	
B-N	56.45	1	56.45	42.53	<0.0001	
C-S	51.50	1	51.50	38.80	<0.0001	
AB	2.94	1	2.94	2.22	0.1548	
AC	6.75	1	6.75	5.09	0.0376	
BC	2.58	1	2.58	1.95	0.1810	
A^2	0.17	1	0.17	0.13	0.7234	
B^2	1.32	1	1.32	0.99	0.3331	
C^2	4.43	1	4.43	3.34	0.0852	
Residual	22.56	17	1.33			
	283.03	26				

were measured from each test specimen. The duties of N, S, and SiC were the UTS and WNH of the UWFSW of AA6061/SiC's UWFSW. Eqs (2) and (3) can be used to describe the response surface, as can Eq. (4), which is a second-order polynomial (regression) [20].

The quadratic model is created first. The ANOVA method is used to identify significant responses and interaction terms. The *F*-statistic is used to determine the significance factor. *p*-value, *F*-value, degree of freedom, the sum of squares, mean sum of squares, coefficient of variation, determination coefficient, adjusted determination coefficient, and other statistical analyses were utilized. The sum of squares obtained from the ANOVA is used to evaluate the percentage of contributions for each component. The properties of independent and dependent variables are learned using ANOVA in a quadratic polynomial equation with both independent and dependent variables. Eqs (6) and (7) are the final regression relations for calculating the UTS and WNH of a UWFS-welded joint for AA6061/SiC:

$$\begin{aligned}\mathrm{UTS} = {} & 161.09418 + 3.70237x\mathrm{A} \\ & - 0.010857x\mathrm{B} + 0.095210x\mathrm{C} \\ & - 2.81977\mathrm{E}-004x\mathrm{A}x\mathrm{B} \\ & - 5.14535\mathrm{E}-003x\mathrm{A}x\mathrm{C} \\ & - 4.00000\mathrm{E}-004x\mathrm{B}x\mathrm{C} - 0.070669x\mathrm{A}\text{^}2 \\ & + 1.13889\mathrm{E}-005x\mathrm{B}\text{^}2 \\ & + 1.30556\mathrm{E}-003x\mathrm{C}\text{^}2\end{aligned} \tag{6}$$

$$\begin{aligned}\mathrm{WNH} = {} & 50.31928 + 0.48867x\mathrm{A} \\ & - 3.60481\mathrm{E}-003x\mathrm{B} - 0.21980x\mathrm{C}\end{aligned} \tag{7}$$

$$+1.88808E-004xAxB-0.011438xAxC$$
$$-1.15979E-004xBxC$$
$$-4.26816E-003xA\hat{}2$$
$$+2.92847E-006xB\hat{}2$$
$$+8.59556E-003xC\hat{}2$$

The ANOVA approach confirms the appropriateness of the final established regression relationships. If the calculated value of the developed model's F-ratio is smaller than the standard F-ratio value from the F table at the specified degree of confidence, it verifies the developed model's acceptability (say 95%) [14, 21].

From the interaction plot shown in Table 4, we find that the interaction of the tool rotating speed and the welding speed of the silicon carbide was not significant (p-value > 0.05), while the interaction between the tool rotating speed and the silicon carbide was significant (p-value < 0.05). Table 5 shows the ANOVA result for the microhardness. From the statistical analysis considering three parameters and three levels, it is evident that all the main effects of the parameters and their interaction effects are not significant to the microhardness as their p-values are >0.05 in a 95% confidence interval.

4.2. Optimization of process parameters

The effect of UWFSW parameters on UTS is represented in the perturbation plot (Figure 6) for an optimized design. From the plot, it is clear that the response changes when each factor moves away from the common or reference points keeping all other factors constant at that reference point. It is also clear from the plot that the tool rotating speed (A) is the most dominating factor on UTS followed by welding speed (B) and SiC (C).

The interaction influences of N, S, and SiC on the UTS are depicted in Figures 7–9. The 2D and 3D contour plots demonstrate the influence of N and S on UTS arising from retaining AA6061/18 SiC (Figures 2A and 2B).

The ideal value of the UTS (MPa) is reached in the center of the contour plot, which is shown as a concentric circle (Figures 2A and 2B). The optimal UTS of 210 MPa is attained at an N of 1,800 rpm and an S of 10 mm/min, as shown in the plot. When the N and S diverge from the specified values, the UTS will tend to drop or grow.

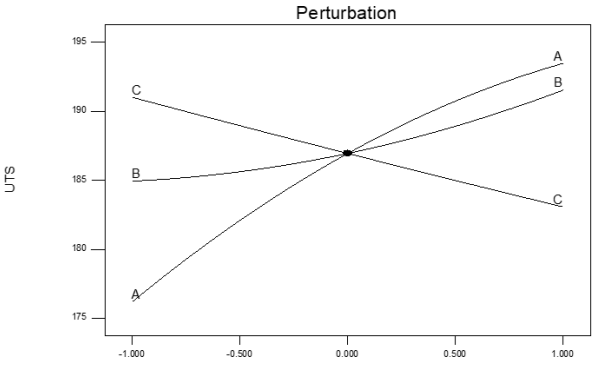

Fig. 6. The influence of UWFSW parameters on the UTS of the UWFSW joint is shown by a perturbation plot

Figure 9 depicts the interaction impact of SiC and S at a constant N of 1,800 rpm. The approximate value of the optimal UTS of 210 MPa is attained at an S of 10 mm/min and a SiC of 18%, as illustrated in the 2D and 3D contour plots.

The perturbation plot (Figure 10) for an optimized design depicts the effect of UWFSW process parameters on WNH. At any operating level of N, WNH should be higher than that of base metal. The microhardness of base metal AA6061/18% SiC is 60.2 HV and it is usually lower compared to the stir zone (60.2 HV). The interaction impact of N, S, and AL on the WNH is depicted in Figures 11–13. Figures 13A and 14B show the effect of N and S on WNH while keeping the SiC constant at 18%.

WNH (HV) is depicted as a concentric ellipse, with the ideal WNH value located in the contour plot's center (Figures 12A and 12B). The ideal WNH of 60.2 HV is attained at an N of 1,800 rpm and an S of 105 mm/min, as illustrated in the plot. Figure 15 depicts the interaction impact of SiC and N at a constant S of 10 mm/min. The optimal WNH is attained around 60.2 HV at an N of 1,800 rpm, as seen in the 2D and 3D graphs. Figure 13 depicts the interaction impact of SiC and S at a constant N of 1,800 rpm. We observe from the 2D and 3D plots that the ideal WNH of 60.2 HV is attained at an S of 10 mm/min and a SiC of 6 kN.

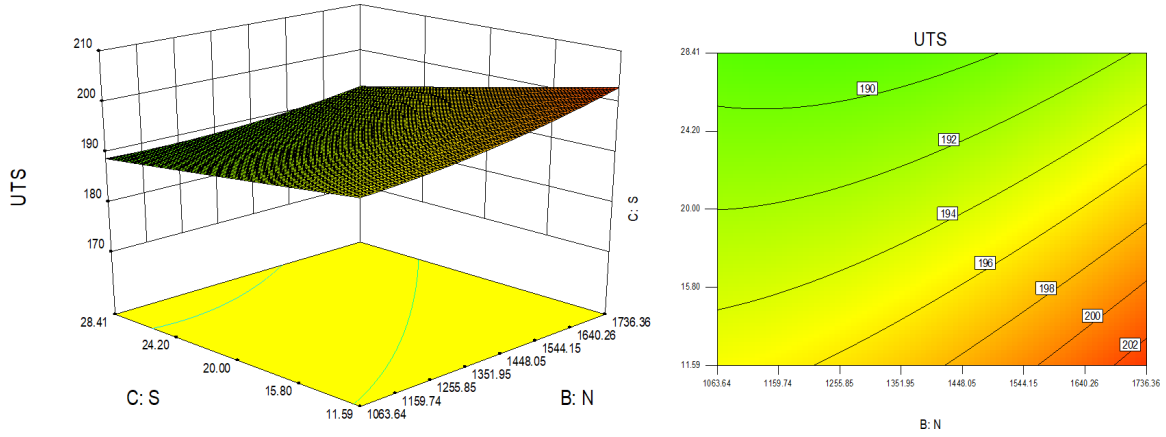

Fig. 7. The influence of N and S on the UTS of the UWFSW joint is represented by contour plots: **(A)** plot of contour 2D; **(B)** plot of contour 3D

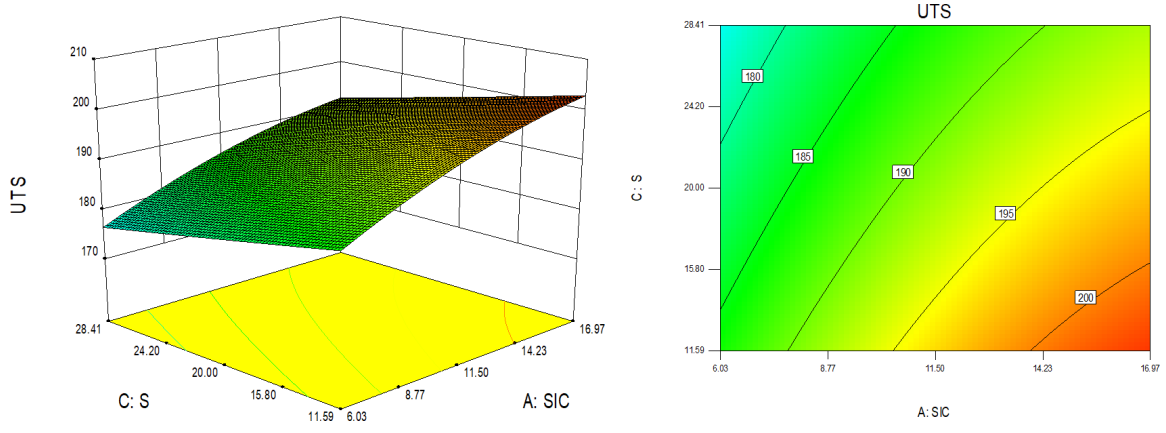

Fig. 8. The influence of SiC and S on the UTS of the UWFSW joint is represented by contour plots: **(A)** plot of contour 2D; **(B)** plot of contour 3D

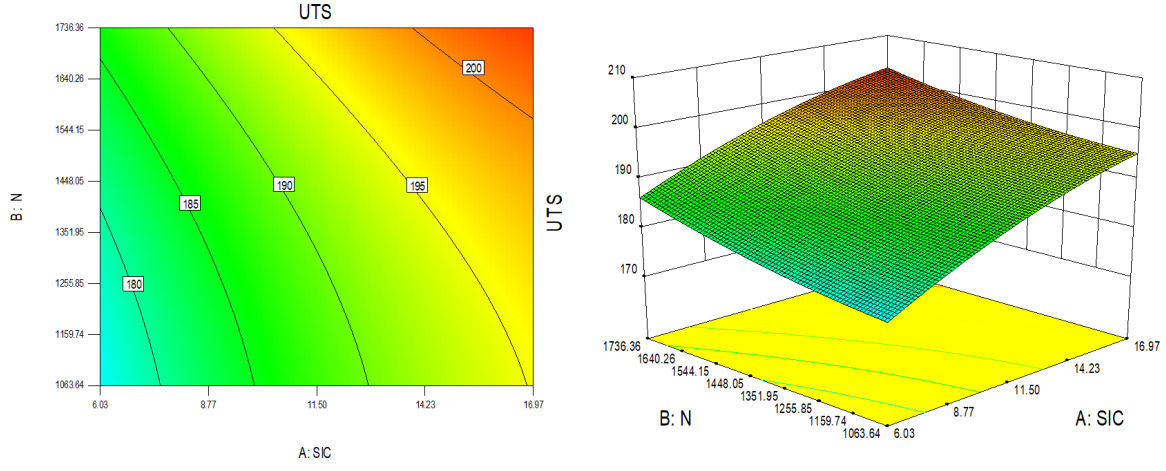

Fig. 9. The influence of N and S on the UTS of the UWFSW joint is represented by contour plots: **(A)** plot of contour 2D; **(B)** plot of contour 3D

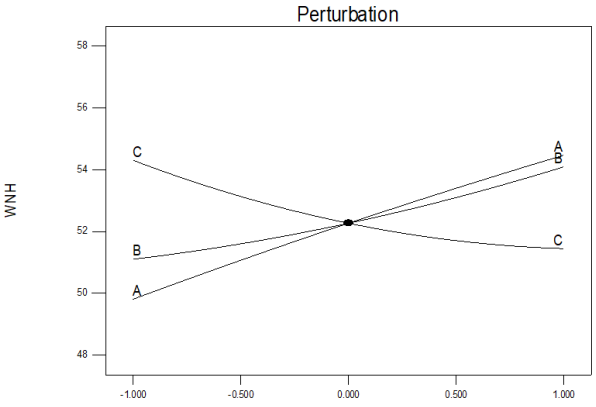

Fig. 10. The influence of UWFSW parameters on the WNH is represented by a perturbation plot

4.3. Modeling validation

The desirability function approach is a widely utilized technique in multiple response optimization. Harrington first presented the desirability function technique in 1965 [14, 20, 21]. This approach determines the optimal operating conditions for obtaining the desired response values. All outputs are translated to individual DFs with a scale factor of between 0 and 1. These functions are organized by initializing the values to be the target, minimum, or maximum output obtained during the experiments. The optimal conditions of UWFSW parameters to maximize hardness and ultimate tensile strength of UWFS-welded Al 6061/5%wt. SiC, Al 6061/10%wt. SiC, and Al 6061/18% SiC were determined using response surface methodology. The optimized UWFSW parameters to maximize hardness and ultimate tensile strength of the weld joint were obtained using a ramp chart and bar chart, as shown in Figure 14. The optimized parameters were N, a rotation speed of 1,736.36 rpm, a travel speed of 11.58 mm/min, and a SiC of 16.67%, with a desirability value of 0.922.

4.4. Validation of the model that has been constructed

The experimental data are used to validate the model created using the desirability technique, and the errors are estimated for all 27 runs, as shown in Table 2. For UTS and WNH, Table 7 shows the actual value, anticipated value, and percentage error. The real values are discovered through trials, and the anticipated values are derived using the Design-Expert software's empirical equations [22–24]. For UTS, the proportion of error ranges from −6.133 to +5.19. WNH's percentage of inaccuracy is similar, ranging from −1.550 to +5.372. As a consequence, the newly created model has predicted UTS and WNH values that are quite similar to the experimental data. The findings of the validation trials are presented in Table 7. The model is also tested for the ideal welding circumstances that are anticipated, with an N of 1,736.36 rpm, an S of 11.59 mm/min, and a SiC of 16.96%.

4.5. Microstructure characterization

Figure 15A depicts the presence of coarse grains in the base composite material (AA6061/18% SiC), as well as the dendritic structure caused by the stir-casting process and SiC particle dispersion in the metal matrix. The macrostructural investigation of the UWFS-welded connection is shown in Figure 17B. In the cross weld microstructure of UWFS-welded MMC joints, the four separate zones of UWFSW, WNZ, TMAZ, HAZ, and unaffected zone (base material), can be seen in Figures 16A–16F.

Due to variable heating and cooling circumstances in UWFSW, it also indicates the presence of diverse microstructure and grain sizes in WNZ, TMAZ, and HAZ. In comparison to the TMAZ, HAZ, and unaffected zones, the weld nugget zone features finer granules. The presence of tiny recrystallized structures in the WNZ is also visible in this photomicrograph. Due to the mechanical stirring action of the UWFSW tool, the coarse grain structure visible in the base composite material (Figure 16A) transforms into a fine grain structure, as seen in Figure 17A–17F. The optical microscopic of the base composite material and the UWFS-welded composite is shown in Figures 16A–16F. The grain size and distribution of SiC in the base composite material (AA6061/18%wt. SiC) are shown in Figure 16A. Figure 16 depicts the existence of the four distinct zones (TMAZ, WNZ, HAZ, and unaffected zone). When compared to the TMAZ, HAZ, and unaffected zone, the WN zone

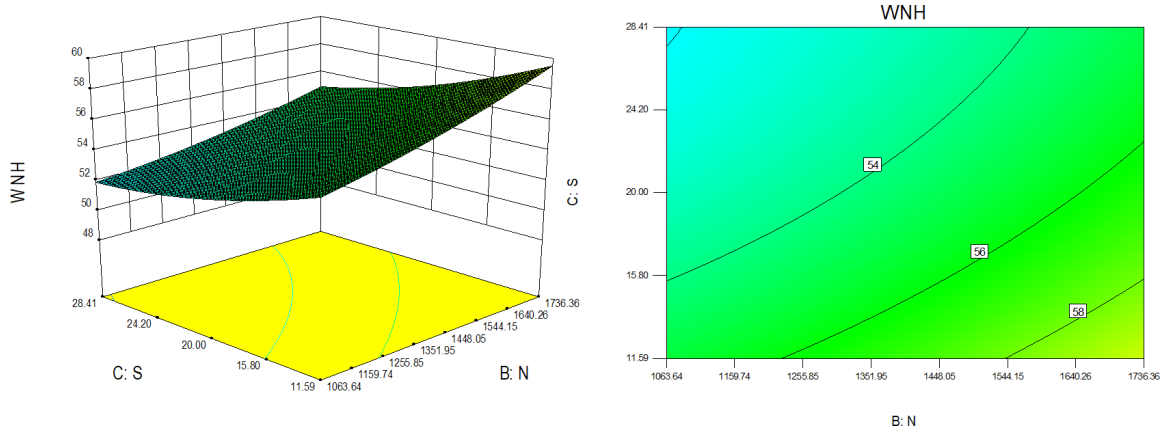

Fig. 11. The influence of N and S on the WNH of the UWFSW joint is represented by contour plots: **(A)** plot of contour 2D; **(B)** plot of contour 3D

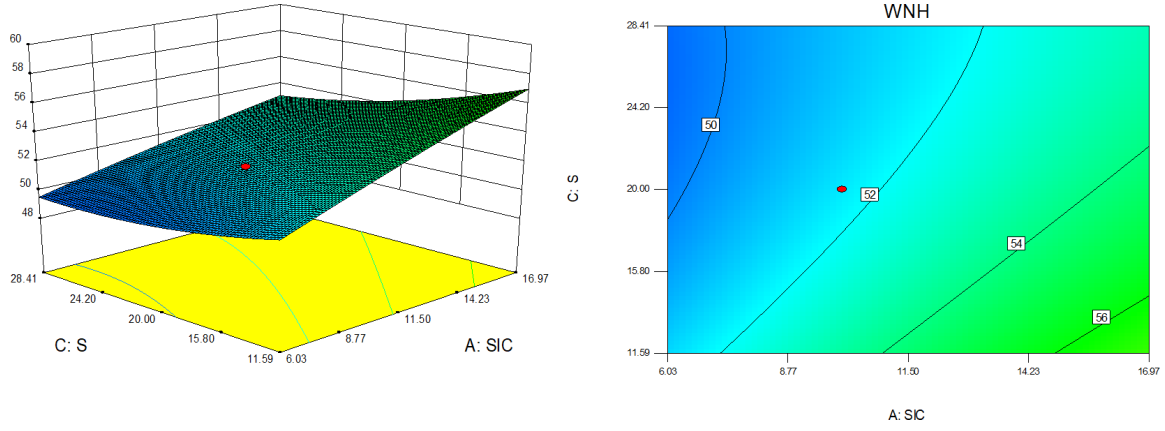

Fig. 12. The influence of SiC and S on the WNH of the UWFSW joint is represented by contour plots: **(A)** plot of contour 2D; **(B)** plot of contour 3D

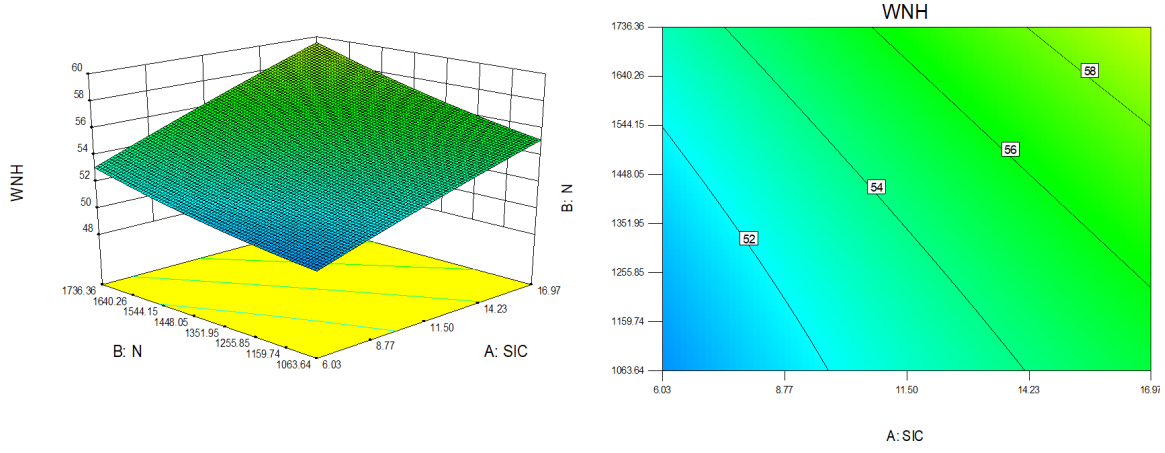

Fig. 13. The influence of N and S on the WNH of the UWFSW joint is represented by contour plots: **(A)** plot of contour 2D; **(B)** plot of contour 3D

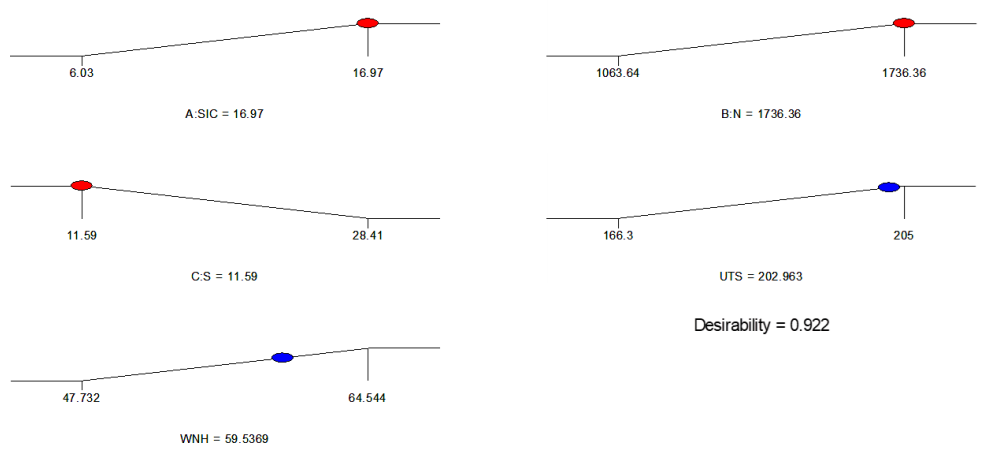

Fig. 14. A graphic that predicts the best UWFSW process parameters

Table 6. The optimization criteria that were applied in this study

Parameters/responses of the process	Goal	The bare minimum	The bare maximum	Significance
A:SiC	Is in range	6.03417	16.9658	3
B:N	Is in range	10,063	1,736.36	3
C:S	Is in range	10	28.409	3
UTS	Maximize	186.3	202.9	3
WNH	Maximize	47.732	64.544	3

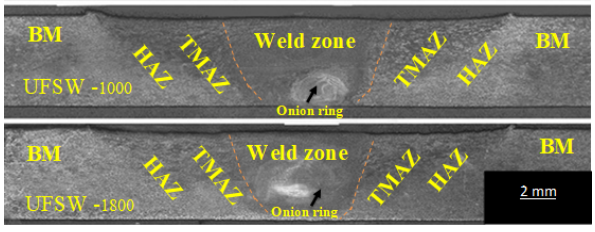

Fig. 15. UWFwelded macrostructure for 6061/18% **(A)** UWFSW at 1,000 rpm **(B)** UWFSW at 1,800 rpm SiC composite

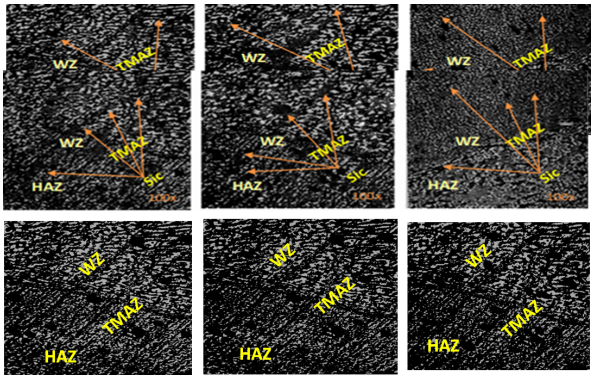

Fig. 16. UWFSW optical microscopic for composite material at 1,000 rpm and 6,061/5%, SiC. **(A)** At 1,000 rpm and 6,061/10%, SiC. **(B)** At 1,000 rpm and 6,061/18%, SiC. **(C)** At 1,800 rpm and 6,061/5%, SiC min. **(D)** At 1,800 rpm and 6,061/10%, SiC. **(E)** At 1,800 rpm, SiC **(F)** and 6,061/18% SiC **(G)** Microstructure of UWFSW for AL6061 at speed 1,000 rpm **(H)** Microstructure of UWFSW for AL6061 at speed 1,400 rpm **(I)** UWFSW for AL6061 at speed 1,800 rpm

possesses a smooth grain structure (Figure 16C–16F). It demonstrates the existence of reinforcing particles (SiC) in the grain borders, which function as a barrier to dendritic development. MMCs' UTS and microhardness improve when dendritic development is reduced. It also illustrates how the degree of cluster aggregation and its expansion with the addition of SiC particles gives MMCs a lot of strength. Following the confirmation of the results, an optical microscope investigation of a cracked tensile specimen of FS-welded (AA6061/18%wt.

Table 7. The outcomes of the experiments as well as the values anticipated by the Design-Expert software for all numbers of runs

n	UTS			WNH		
	Actual UTS	**Predicted UTS**	**Error%**	**Actual WNH**	**Predicted WNH**	**Error%**
1	205.000	204.909	0.091	64.544	59.172	5.372
2	196.000	192.538	3.462	55.243	55.779	−0.536
3	190.000	184.806	5.194	52.942	53.658	−0.716
4	200.000	200.218	−0.218	55.980	57.530	−1.550
5	190.000	187.846	2.154	53.679	54.137	−0.458
6	180.000	180.114	−0.114	51.378	52.017	−0.639
7	190.000	195.526	−5.526	55.198	55.888	−0.690
8	185.000	183.154	1.846	52.897	52.496	0.401
9	174.000	175.422	−1.422	50.596	50.375	0.221
10	202.000	200.937	1.063	56.113	57.431	−1.318
11	186.400	188.566	−2.166	53.812	54.038	−0.226
12	174.700	180.833	−6.133	51.511	51.917	−0.406
13	195.300	196.245	−0.945	54.548	55.789	−1.241
14	183.700	183.874	−0.174	52.247	52.396	−0.149
15	172.300	176.142	−3.842	49.946	50.276	−0.330
16	193.100	191.554	1.546	53.766	54.147	−0.381
17	180.030	179.182	0.848	51.465	50.755	0.710
18	170.320	171.450	−1.130	49.164	48.634	0.530
19	196.000	196.965	−0.965	56.113	55.690	0.423
20	185.100	184.593	0.507	52.380	52.297	0.083
21	176.200	176.861	−0.661	50.079	50.177	−0.098
22	191.300	192.273	−0.973	53.117	54.048	−0.931
23	184.200	179.902	4.298	50.816	50.655	0.161
24	171.200	172.169	−0.969	48.515	48.535	−0.020
25	187.100	187.582	−0.482	52.335	52.406	−0.071
26	181.100	175.210	5.890	50.034	49.014	1.020
27	166.300	167.478	−1.178	47.732	46.893	0.839

SiC) MMC with optimal settings was performed. The optical microscope report of the microstructure of the broken tensile specimen is shown in Figures 16A–16F. It clearly distinguishes between a non-fractured and a fractured surface area.

The high-resolution optical micrographs and the XRD patterns of the prepared AMCs are shown in Figures 16 and 17, respectively. The diffraction peaks of SiC, which represent the major elements of the SiC particles, are distinctly identified. The intensities of the peaks rise as SiC content within the matrix increases. It is noticed in Figure 17 that the diffraction peaks of aluminum in the composites are slightly shifted to lower 2θ compared to that of the base alloy due to the addition of SiC particles in the aluminum matrix. It is obvious from Figure 17 that there are no other diffraction peaks detected except the peaks for elements Al, SiC. This observation leads to a conclusion that during the casting of AMCs, the integrity of SiC particles was conserved. At the processing temperature of compo casting, SiC particles are thermodynamically stable. The occurrence of any interfacial reaction between fly ash particles and aluminum matrix during casting has not been observed. Such interfacial reactions in the composites would often result in the formation of brittle intermetallic compounds and degrade their significant properties. A wider zone of interfacial reaction and consequently the formation of brittle $MgAl_2O_4$ spinal were observed at the interface of aluminum–fly ash in A356/fly ash AMC prepared by stir casting, as reported by Rajan et al. [25].

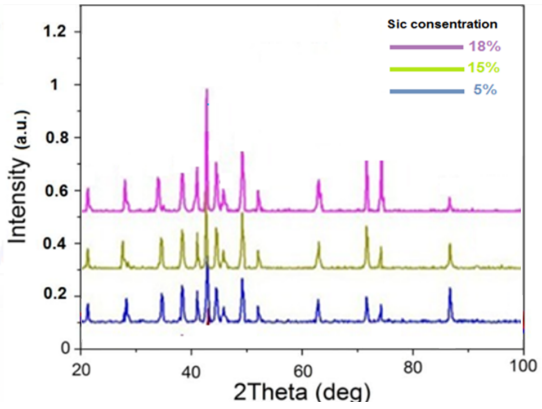

Fig. 17. XRD patterns of AA6061/SiC with different content of SiC particles

5. Conclusions

In the present study, the effect of UWFSW parameters such as tool rotating speed, welding speed, and silicon carbide on ultimate tensile strength and microhardness of Al 6061/5%wt., Al 6061/10%wt., and Al 6061/18%wt. welded joint was investigated in detail. Response surface methodology was used to design the experiment, optimize, and predict outputs. The parameters' effect (linear, interaction, and square) and their significance were determined using the response surface methodology.

1. The input parameters are significant for ultimate tensile strength and microhardness. Tool rotating speed is the most significant parameter, followed by welding speed and then silicon carbide. The interactions of tool rotating speed to welding speed and silicon carbide are significant, but the interaction between welding speed and silicon carbide is not significant.
2. The association amidst the responses (UTS and WNH) and input parameters (N, S, and SiC) has been effectively developed using the Box–Behnken experimental design. Three values have been chosen for each parameter, and tests have been conducted to optimize the UTS and WNH.
3. The interaction effects of welding parameters are investigated using perturbation plots, 2D and 3D contour plots, and perturbation graphs. The most influential parameter is N. At welding circumstances of N 1,736.36 rpm, S 11.58 mm/min, and SiC 16.67%, the apt UTS and WNH are determined to be 202 MPa and 59.5339 HV, respectively.
4. The results of all 27 tests designed using the Box–Behnken method are effectively applied to the desirability approach. At the matching welding circumstances of 1,736.36 rpm N, 11.58 mm/min S, and 16.67% SiC, the optimal values achieved are 202.59 MPa for UTS and 59.5339 HV for WNH.
5. By comparing the outcomes of all 27 trials with projected results for the same welding setting, the newly constructed model is verified for UTS and WNH. UTS has a maximum percentage error of −6.133 and WNH has a maximum percentage error of −1.550. The newly created model correctly predicted UTS and WNH values that were highly similar to the experimental data.
6. When compared to TMAZ, HAZ, unconstrained zone, and base AMC, microstructural characterization of UWFSW joints indicated that the WN zone had a smooth grain structure.

References

[1] El-Kassas AM, Sabry I. An appraisal of characteristic mechanical properties and microstructure of friction stir welding for Aluminium 6061 alloy – Silicon Carbide (SiCp) metal matrix composite. J Mech Eng Sci. 2019;13:5804–17.
[2] H. A. K. A. Khaki S. Int J Adv Design Manuf Technol. 2019;12:25.
[3] Sabry I, El-Kassas AM. Cost estimation of pipe friction stir welding. Int J Adv Res Innov. 2017;4:121–7.
[4] El-Kassas A, Sabry IRS, Thekkuden DT. Characteristics of potential sources – vertical force, torque and current on penetration depth for quality assessment in friction stir welding of AA 6061 pipes. Int Rev Aerosp Eng. 2019;12:4.
[5] Sabry I, El-Kassas A, Mourad A-HI, Thekkuden DT, Qudeiri JA. Friction stir welding of T-joints: experimental and statistical analysis. J Manuf Mater Process. 2019;3:38.

[6] Wahid MA, Khan ZA, Siddiquee AN. Review on underwater friction stir welding: a variant of friction stir welding with great potential of improving joint properties. Trans Nonferrous Met Soc China. 2018;28:193–219.

[7] Sabry I, Mourad A-HI, Thekkuden DT. Comparison of mechanical characteristics of conventional and underwater friction stir welding of AA 6063 pipe joints. Int Rev Aerosp Eng. 2020;14:1.

[8] Sabry I, El-Zathry NE, El-Bahrawy FT, Abdel Ghaffar A. Extended hybrid statistical tools ANFIS-GA to optimize underwater friction stir welding process parameters for ultimate tensile strength amelioration. In: 3rd Novel Intelligent and Leading Emerging Sciences Conference (NILES), Egypt, 2021. https://doi.org/10.1109/NILES53778.2021.9600552

[9] Sabry I, Allah N, Nour M, Ghafaar M. Mechanical characteristic of Al 6063 pipe joined by under water friction stir welding. Adv Sustainability Sci Technol. 2021;9:689–99.

[10] Sabry I, Zaafarani N. Dry and underwater friction stir welding of AA6061 pipes – a comparative study. In: IOP Conf. Series: Materials Science and Engineering. 2021;1091:012032.

[11] Sabry I, Gadallah N, Abdel Ghafaar M, Abdel-Mottaleb MM. Optimization of process parameters to maximize ultimate tensile strength and hardness of underwater friction stir welded aluminium alloys using fuzzy logic. Mod Concepts Mater. 2020;3:73–8.

[12] El-Kassas AM, Sabry I. Optimization of the underwater friction stir welding of pipes using hybrid RSM-fuzzy approach. Int J Appl Eng Res. 2019;14:4562–72.

[13] Wang Q, Zhao Z, Zhao Y, Yan K, Zhang H. The adjustment strategy of welding parameters for spray formed 7055 aluminum alloy underwater friction stir welding joint. Mater Des. 2015;88:1366–76.

[14] Sabry I, Mourad A-HI, Thekkuden DT. Optimization of metal inert gas welded aluminium 6061 pipe parameters using analysis of variance and grey relational analysis. SN Appl Sci. 2020;2:175.

[15] Jandaghi MR, Badini C, Pavese M. Dissimilar friction stir welding of AA2198 and AA7475: effect of solution treatment and aging on the microstructure and mechanical strength. J Manufacturing Process. 2020;57:712–24.

[16] Jandaghi M, Pouraliakbar H, Saboori A, Hong SI, Pavese M. Comparative insight into the interfacial phase evolutions during solution treatment of dissimilar friction stir welded AA2198-AA7475 and AA2198-AA6013 aluminum sheets. Materials. 2021;14:1290–9.

[17] Jandaghi M, Pouraliakbar H, Hong SI, Pavese M. Grain boundary transition associated intergranular failure analysis at TMAZ/SZ interface of dissimilar AA7475-AA2198 joints by friction stir welding. Mater Lett. 2020;280:128557.

[18] Sabry I. Investigation of microstructure and mechanical characteristic of underwater friction stir welding for Aluminum 6061 alloy – Silicon carbide (SiC) metal matrix composite. J Mech Eng Sci. 2021;15:8644–8.

[19] Sabry I, Thekkuden, DT, Mourad, A-HI, Khan SH. Optimization of tungsten inert gas welding parameters using grey relational analysis for joining AA 6082 pipes. In: 2022 Advances in Science and Engineering Technology International Conferences, 2022.

[20] Sabry I, Thekkuden DT, Mourad A-HI, Abdullah K. Variants of friction stir welding for joining AA 6063 pipes. In: 2022 Advances in Science and Engineering Technology International Conferences (ASET), 2022:1–4. https://doi.org/10.1109/ASET53988.2022.

[21] Thekkuden DT, Mourad A-HI, Sabry I. TOPSIS – GRA approach to optimize friction stir welded aluminum 6061 pipes parameters. In: 2022 Advances in Science and Engineering Technology International Conferences (ASET), 2022:1–6. https://doi.org/10.1109/A, 2022.

[22] Sabry I. Experimental and statistical analysis of possibility sources – rotation speed, clamping torque and clamping pith for quality assessment in friction stir welding. Manag Prod Eng Rev. 2021;12:83–96.

[23] Sabry I, Mourad A-HI, Thekkuden DT. Vibration-assisted friction stir welding of AA2024-T3 plates. In: Proceedings of the ASME 2021 Pressure Vessels & Piping Conference PVP2021 July 12–16, 2021, Virtual, Online, 2021.

[24] Sabry I, Mourad A-HI, Thekkuden DT. Study on underwater friction stir welded AA 2024-T3 pipes using machine learning algorithms. In: Conference: ASME 2021 International Mechanical Engineering Congress and Exposition, 2021. https://doi.org/10.1115/IMECE2021-71378

[25] Rajan TPD, Pillai RM, Pai BC, Satyanarayana KG, Rohatgi PK. Fabrication and characterization of Al-7Si-0.35Mg/fly ash metal matrix composites processed by different stir casting routes. Composites Sci Technol. 2007;67:3369-77.

Received 2022-02-23
Accepted 2022-05-09